ASTRONOMY & ASTROPHYSICS
SUPPLEMENT SERIES

AUGUST **1998**, PAGE 197

Astron. Astrophys. Suppl. Ser. **131**, 197-208 (1998)

F, G and K stars in the ROSAT all-sky survey⋆,⋆⋆

I. Photometry

A.D.F. Metanomski[1,2], L. Pasquini[2], J. Krautter[1], G. Cutispoto[3], and T.A. Fleming[4,5]

[1] Landessternwarte Heidelberg, Königstuhl, D-69117 Heidelberg, Germany
[2] European Southern Observatory, Alonso de Cordova 3107, Vitacura, Santiago, Chile
[3] Osservatorio Astrofisico di Catania, v.le A. Doria 6, I-95125 Catania, Italy
[4] Max-Planck-Institut für Extraterrestrische Physik, Karl-Schwarzschild-Str. 2, D-85740 Garching, Germany
[5] Steward Osbervatory, University of Arizona, Tucson, AZ 85721, U.S.A.

Received May 20; accepted December 9, 1997

Abstract. We present accurate $BV(RI)_{\rm c}$ photometry for a sample of F, G and K stars detected in selected areas of the ROSAT all-sky survey (RASS). We have used the photometry, in addition to low-resolution spectroscopy, to estimate spectral classifications, distances and X-ray luminosities. The $\log(L_{\rm X}/L_V)$ in the sample lies below -2. Although the sample contains also nearby, inactive stars, it is dominated by active objects. The median X-ray luminosity in our sample is $< L_{\rm X} >= 29.88$ and the mean value of the hardness ratios $<$ HR1 $>= 0.13 \pm 0.35$.

We compare the derived X-ray luminosity function with similar functions obtained from the serendipitous samples of the Einstein Observatory medium sensitivity survey (EMSS) and EXOSAT.

Our sample is completely consistent with the EMSS sample of solar type stars, indicating that both our sources and the EMSS sources are representative of the high galactic latitude X-ray stellar population. We do not find extremely active stars ($\log(L_{\rm X}) \geq 32$), as are found in the EMSS sample, and we argue that these objects are rare.

Key words: stars: late-type — X-ray: stars — surveys

1. Introduction

With the launch of the first imager X-ray satellite, Einstein, X-ray emission was detected from stars of nearly all spectral types (see for example Vaiana et al. 1981; Pallavicini 1989). In addition to the data obtained by using pointed observations, a large body of information on the coronae of late-type stars came from the study of serendipitously detected stars, both in the Einstein EMSS and the EXOSAT surveys. Results on stellar coronae are summarized in numerous reviews (i.e. Pallavicini 1989; Vaiana 1990; Linsky 1990). Late-type stars show a large spread in their X-ray luminosities (up to 3 orders of magnitudes), which correlate with stellar rotational velocities ($L_{\rm X} \propto v \sin i^2$, Pallavicini et al. 1981).

Up to now, the largest sample of X-ray selected late-type stars came from the EMSS survey. This sample consists of a total of 169 solar type stars, out of which 128 were studied by Fleming (1988, also Fleming et al. 1989). Fleming's results confirm the correlation between X-ray luminosity and rotational velocity for solar-type single stars, although he finds a different correlation ($L_{\rm X} \propto v \sin i$) to the one found by Pallavicini et al. (1981). He also found evidence for a saturation of the X-ray emission. This saturation would represent a maximum level of X-ray emission for solar-type stars, corresponding to a surface flux of $F_{\rm X} \sim 7\ 10^7$ erg s^{-1} cm^{-2}.

Since the launch of the ROSAT satellite (Trümper 1992) with its all-sky survey (RASS), larger samples are available. The ROSAT PSPC passband, $0.1 - 2.4$ keV, is different from the Einstein IPC ($0.3 - 3.5$ keV). It is therefore necessary to investigate the nature of the coronal sources in the RASS and to compare their characteristics with those from the pre-ROSAT era.

In this work we present the results of photometric observations of solar-type stars detected in the RASS. Spectral classification obtained from the colours is presented, as well as the distance and X-ray luminosity estimates derived from this classification. Our results are compared with those obtained from the Einstein and EXOSAT

Send offprint requests to: A. Metanomski,
e-mail: ametanom@mail.lsw.uni-heidelberg.de

⋆ Table 3 is also available in electronic form at the CDS via anonymous ftp to cdsarc.u-strasbg.fr (130.79.128.5) or via http://cdsweb.u-strasbg.fr/Abstract.html

⋆⋆ based on observations collected at ESO, La Silla.

surveys. We finally aim at defining selection criteria for solar-type stars, in order to allow automatic searches of the RASS database.

2. Sample and observations

2.1. The sample

The RASS was conducted from August 1990 until January 1991, with supplemental observations taken in February and August 1991. The 2 PSPCs on board ROSAT were the instruments in use for the entire RASS. Descriptions of the observing methods employed during the survey, as well as the data reduction techniques, can be found in Cruddace et al. (1991).

The raw PSPC survey data were processed automatically using the ROSAT Standard Analysis Software System (SASS). The SASS time-tagged, gain-corrected, and applied an attitude solution to each detected X-ray photon. During the first processing of the RASS data, the SASS was also used to compile a first-cut catalogue of RASS sources (Voges 1992). A maximum likelihood (ML) algorithm was run automatically on the RASS data to find all X-ray sources above a likelihood threshold of 11. The source detection algorithms were run on images of different energy bands so that the hardness ratios could be computed for all sources.

In order to calibrate various methods for identifying the contents of the RASS, it was decided to identify all RASS sources in four fields, covering a 575 square degree area of the sky, using optical spectroscopy in a manner similar to the EMSS (Stocke et al. 1991). Telescope time for this project was granted under a Key program at ESO and four study areas were chosen at high Galactic latitude on the southern sky (Danziger et al. 1990).

In order to identify the optical counterparts of the X-ray sources, low-resolution (7 Å and 16 Å) spectra of the objects inside the error circle of the X-ray position were taken, using the Boller&Chivens spectrograph at the ESO 1.5 m telescope and the EFOSC1 in spectrographic mode at the 3.6 m telescope at La Silla. Spectra of bright stars were acquired even if the objects were situated outside of the error circle. The spectra were used to perform a first spectral classification.

For some of the F, G and K stars, intermediate (2 Å) resolution spectra of the Hα line were obtained in order to confirm the likely coronal source, through the presence of enhanced chromospheric activity.

Out of the complete sample of RASS sources, the "solar" type (A to K) stars were selected and are presented in this work. A total of 107 A-K stars were found, out of ∼600 sources.

Table 1. Observing periods

Dates	Detector
21 Apr ÷ 02 May 1994	EMI 9658R
01 Oct ÷ 10 Oct 1994	EMI 9658R
02 Nov ÷ 12 Nov 1995	Hamamatsu
06 May ÷ 16 May 1996	Hamamatsu

2.2. The photometric observations

The photometric observations were carried out at the European Southern Observatory at La Silla, using the 0.5 m ESO telescope, equipped with a single-channel photon-counting photomultiplier, and the standard ESO $BV(RI)_{\rm c}$ filters. The available U filter was not used, due to the fact that our sample stars are red and for the most rather faint, so that the low counts in the U filter would have led to inaccurate data. Two photomultipliers were used, a red-sensitive dry-ice cooled EMI 9658 and a Peltier-cooled Hamamatsu GaAs (see Table 1).

Each measurement consisted normally of three 10 s integrations in each filter. For the faintest stars, longer integration times of $20 - 30$ s were used. The transformation coefficients were obtained by observing Cousin's E-region standard stars. Atmospheric extinction coefficients were obtained by observing two E-region standards of very different spectral types at different airmasses during the night.

The errors are of the order 0.01 mag in all filters for stars brighter than $V = 12$. For stars fainter than $V = 12$, the errors are higher, of the order 0.03 in the V, R, and I filters and 0.04 in the B filter. The results of the observations are listed in Table 3.

Stars brighter than $V = 5.5$ (four of our sources) were not observed, as they were too bright for either photomultiplier tube used. For these stars, we have taken the spectral classification, as well as the photometric data, from the literature. These data are also given in Table 3.

2.3. Spectral classification

The photometric data were used to determine the spectral type and luminosity class of our sample objects, as a complement to the classification already done using the low-resolution spectra available from the identification program.

The photometric spectral classification was done using the colour tables computed by Cutispoto et al. (1996). These tables contain mean values of the colour indices for stars in the spectral range A to K. For each of our sources, a combination of spectral type and luminosity class were selected, by comparing the data with the synthetic colours. The results are summarized in Table 3.

In case that no single star would fit the observations, the object was considered a binary. The observed colours

were then compared with the results of the combinations of two single stars, and the combination that best reproduced the data was selected. The results were checked with the help of high-resolution spectra, also obtained in the course of our program (see Metanomski et al. 1997a,b). In most cases, the spectra confirmed the binarity of the source.

We would like to note that this procedure assumes unreddened stars with normal colours, a reasonable assumption, considering that all our stars are found to be close to the Sun. Distant stars, PMS objects and stars with a high activity level could have significantly altered colours.

In Table 3 are also listed the spectral classifications we had either from the literature and SIMBAD database, or from the low-resolution spectra taken in the course of the identification program. In most cases the spectral classification obtained from the colour indices agrees very well with the available spectral classification. The colour indices also gave binary classification in all cases where an object from the sample was known either from the literature or from spectroscopic observations to be a binary. This method cannot, however, give a correct result if the components of a binary system are very similar. We have in some cases used the information taken from our high resolution spectroscopic observations, if an SB2 system was clearly present. In Table 3 visual, photometric and spectroscopic binaries are separately labeled.

2.4. X-ray fluxes, distances and X-ray luminosities.

To determine the X-ray fluxes from the ROSAT countrates, a conversion factor was adopted from Fleming et al. (1995), appropriate for coronal sources:

$$CF = (8.31 + (5.30 \cdot \mathrm{HR1}))\ 10^{-12}\ \mathrm{erg\ cm^{-2}\ count^{-1}}. \quad (1)$$

The hardness ratio HR1 is defined as:

$$\mathrm{HR1} = \frac{CR\,[ch52 - 201] - CR\,[ch11 - 41]}{CR\,[ch11 - 240]}$$

$CR\,[cha - b]$ being the countrate in the channels "a" to "b".

Since most of the stars in our sample are closer than 200 pc, extinction can be considered negligible, allowing the use of this relation.

The error for the X-ray flux is determined by both the errors on the countrate and the hardness ratio. Depending on the source's intensity, the uncertainty in the X-ray flux can be as high as a factor 2, due mainly to the error in the HR1.

For five of the sources, the X-ray counts obtained were so low, that the objects could only be seen when summing up all channels. For these objects there is no value for the HR1. For these stars we used the mean value of the hardness ratio to determine the X-ray flux, as was done by Fleming et al. (1995).

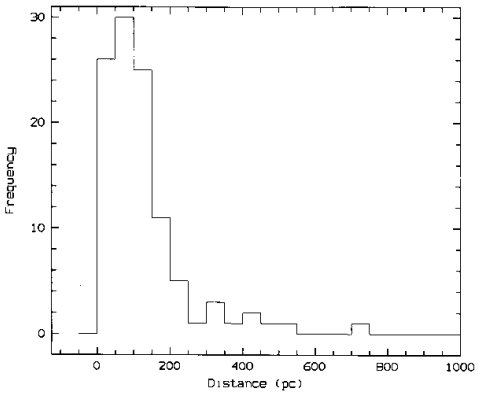

Fig. 1. Distribution of the distances for our sample

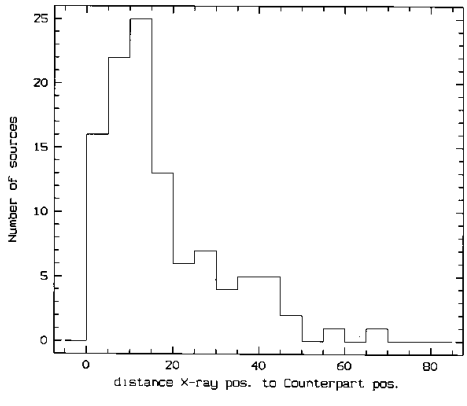

Fig. 2. Distribution of the separation between X-ray and Counterpart positions

The distances were calculated by determining the absolute visual magnitude of the objects, using the observed $(B - V)$ colour indices for single stars, and the spectral types for binaries. The values of M_V as a function of $(B - V)$ were taken from Gliese (1982) or from the lists of Cutispoto et al. (1996), for the early stars and giants/subgiants.

The error in the distance is mainly determined by the error in the $(B - V)$ index for the single stars. This error varies from 0.02 to 0.07 for the faintest objects, leading to an error of 5 to 23% in the distance. For the binaries, an error of one spectral class per component was assumed, leading to an error of up to 30%.

Also to be considered is that for the distance estimation we have used only the photometric spectral classification. This method, as already pointed out in the previous section, assumes "normal" stars with unreddened colours, and does not allow the identification of PMS objects, nor the correct classification of highly active stars. As a PMS nature or the activity level will only be determined with the help of high-resolution spectroscopic observations, the distances for some of our objects may need to be revised at a later time. We would like to note, however, that this

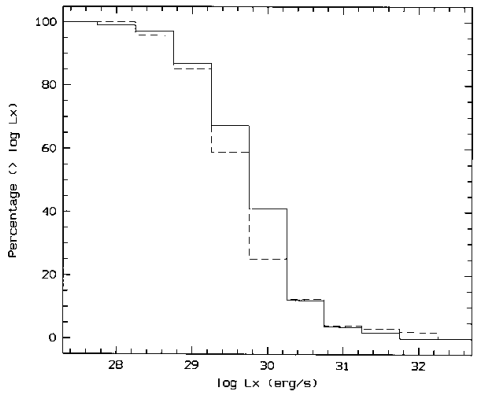

Fig. 3. Cumulative distributions of X-ray luminosities for our RASS sample (continuous line) and the EMSS sample (broken line) as taken from Fleming (1988 and 1995)

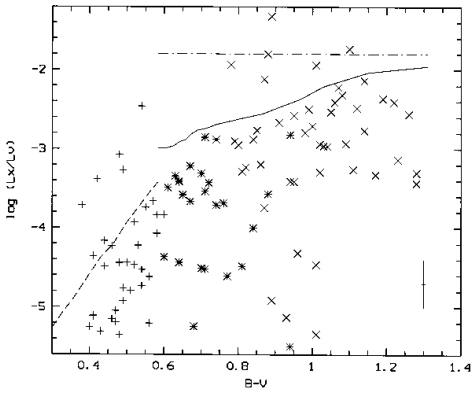

Fig. 4. The X-ray to visual luminosity as a function of spectral type, represented here by the $(B-V)$ colour index. The F stars are represented with (+), the G stars with (∗) and the K stars with (X).The continuous line represents the saturation level of $F_{\rm X} \sim 7\ 10^7$ erg s^{-1} cm^{-2} detected by Fleming in his sample (Fleming 1988). The dashed line is the upper limit for $L_{\rm X}$ as calculated by Vilhu & Walter (1987). The dash-dot line is a constant $\log(L_{\rm X}/L_V)$ of -1.8

method is consistent with the one used for the EMSS and EXOSAT surveys.

3. Results

3.1. Characteristics of sample

The distribution of the distances for our objects is shown in Fig. 1. It is clear that most of our sources lie within 200 pc from the Sun (86% of our sample). Only 15 stars (14% of the sample) lie at distances greater than 200 pc, with only one star as far out as ∼700 pc.

Figure 2 shows the distribution of the separation between the optical counterpart position and the ROSAT X-ray position. Most of the optical counterparts lie at 30″ or less from the X-ray position. Voges (1993) determined that for the RASS 68% of the optical counterparts are within 20″ of the X-ray position. In our sample, 72% lie within that distance, in excellent agreement with Voges' results.

Both the errors in X-ray flux and distance contribute to the uncertainty in the X-ray luminosity, the flux error giving the major contribution. The error for $L_{\rm X}$ is typically about a factor 2.

Figure 3 shows the cumulative X-ray luminosity function for our sample. Although nearly all objects are clearly active, none displays extremely high activity with high X-ray luminosity ($\log(L_{\rm X}) \geq 32$). The median value of the X-ray luminosity is $\log(L_{\rm X}) = 29.88$. This value is higher by two orders of magnitude than the $\log(L_{\rm X})$ observed for the active Sun. 63% of the sample has X-ray luminosity of $\log(L_{\rm X})$ between 29.5 and 30.0. We only have four objects so far with $L_{\rm X}$ of the order of 10^{31} erg s^{-1}.

The X-ray to visual luminosity as a function of spectral type is shown in Fig. 4. Noticeable is the spread in $L_{\rm X}/L_V$ in every spectral class, a spread that is larger than the uncertainty in X-ray luminosity. This spread shows

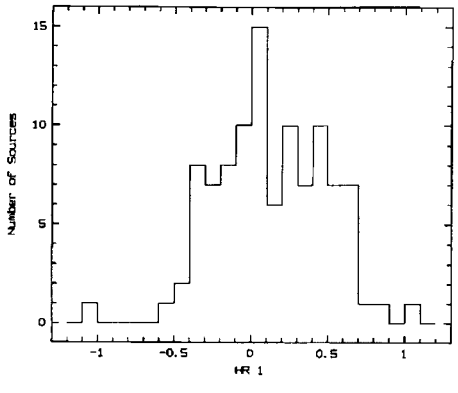

Fig. 5. The distribution of the hardness ratio in our sample. Most sources have hardness ratios between -0.5 and 0.7

the range of activity levels present in the observed objects. For $(B-V) \leq 0.64$, $L_{\rm X}/L_V$ is confined to less than 10^{-3}, with one source only, a binary (F8V+G4V), having a higher value. For $(B-V) \geq 0.64$, the maximal value of $\log(L_{\rm X}/L_V)$ rises to ~ -1.8. Only one source shows a higher value of $L_{\rm X}/L_V$, and that source is so far a good candidate for a PMS object. The turning point value of $(B-V)$ corresponds to the value found by Fleming (1988), where the stars show a constant maximum value of $F_{\rm X} \sim 7\ 10^7$ erg s^{-1} cm^{-2}. For the stars with a bluer $(B-V)$, Fleming finds that the maximal value of $F_{\rm X}$ (or $L_{\rm X}$) rises with later spectral types, as calculated by Vilhu & Walter (1987). The corresponding limiting $\log(L_{\rm X}/L_V)$ (for main-sequence stars) are shown in Fig. 4: the values of Vilhu and Walter by a dashed line, Fleming's maximal value for the surface flux by a

continuous line. Also plotted is a line for $\log(L_X/L_V) = -1.8$. Most of our stars seem to confirm Fleming's maximal value for $F_X \sim 7\ 10^7$ erg s^{-1} cm^{-2}. There are only a few objects above this limit. The nature of these sources with high X-ray surface flux will be investigated further once high resolution spectroscopic observations are available and have been analyzed.

Also of note in the plot is the absence of any low-activity objects in the late-K types (for spectral types later than K4). The reason for this absence of low-luminosity objects is most probably the detection limit of the RASS, which lies at a flux of $f_X \sim 2\ 10^{-13}$ erg s^{-1} cm^{-2}. This means that late K stars with $\log(L_X/L_V) = -4$ (or $\log(L_X) \sim 28.5$) can only be observed if they lie within 36 pc of the Sun, and those with $\log(L_X/L_V) = -5$ (or $\log(L_X) \sim 27.5$) only up to a distance of 10 pc. A study of nearby (≤ 7 pc) K stars made by Schmitt et al. (1995) has shown that high X-ray luminosity is not very frequent among late K stars. The sample they studied contained only 43% of stars of spectral type K4 or later with an X-ray luminosity of $\log(L_X) \geq 27$, and only 27% have $\log(L_X)$ of 27.5 or higher, making them detectable with the RASS at distances of ∼10 pc. In our studied areas there are only 15 K stars belonging to the Gliese catalogue and of spectral type K4-K7. Out of these only two lie within 10−11 pc and another two lie within 12 pc. Therefore, according to the Schmitt and Fleming statistics, we would expect to detect at the most one of these nearby K stars, and this produces the observed gap in Fig. 4.

The distribution of the hardness ratio for the ROSAT sample is given in Fig. 5. Clearly, most of our stars have HR1 values between −0.5 and 0.7. The mean value of the hardness ratio lies near 0, being $< HR1 > = 0.13 \pm 0.35$. Three stars have very high HR1 values and only one has value smaller than −0.5, RXJ 0440.3−5856, with HR1 = −1.05. Such a soft X-ray emission is usually characteristic of white dwarfs. The counterpart for this source, though, is a wide binary composed of two dwarf G-stars. In this case we have rather a X-ray quiet source ($\log(L_X) = 28.2$), which may explain the soft spectrum. Another possibility is that we have a binary system with a white dwarf companion.

3.2. Selection criteria

Considering the large amount of sources (∼60 000) that compose the RASS catalogue, an automated search for objects of interest, using for instance the guide Star Catalogue, would be of definite advantage. For this reason, we have tried to determine good selection criteria for solar-type stars using our sample.

First of all, the considered objects should be close to the X-ray position, at maximum 20″ distance. 72% of our objects lie within this radius of the X-ray position. The optical sources should be brighter than 15 mag in the visual range.

Table 2. Distribution of our sources among the spectral types F, G and K, as well as distribution in the EMSS and EXOSAT samples

Source type	our sample		EMSS data		EXOSAT data	
	Num.	Perc.	Num.	Perc.	Num.	Perc.
A stars	1	1%	5	3%	2	7%
F stars	34	32%	51	30%	5	18%
G stars	24	22%	45	27%	13	46%
K stars	48	45%	68	40%	8	29%

The hardness ratio for our sources is mostly between −0.4 and 0.7. 92% of the stars have a HR1 included in this interval. So in an automated search only X-ray sources with HR1 between these two values should be considered.

The X-ray flux of the ROSAT source can be calculated using either a constant conversion factor for the countrates, or the formula given by Fleming et al. (1995) and used in this work (see Eq. 1). Since a high photometric accuracy is not required for a first selection, candidates can be directly selected, and their approximate visual flux determined, from existing large surveys. The ratio of X-ray to visual flux determined using these values should not exceed $\log(f_X/f_V) = -3$ for F stars and early G stars ($(B-V) \leq 0.64$), and $\log(f_X/f_V) = -1.8$ for later spectral types ($(B-V) > 0.64$).

3.3. Comparison with EMSS and EXOSAT samples

Table 2 lists the distribution of our sources, as well as for the sources from the EMSS and EXOSAT surveys, between the spectral types A, F, G and K (including the primaries of binary systems, for which the secondaries have not been included). The EMSS sample has been taken from Stocke et al. (1991) and the EXOSAT sample from Cutispoto et al. (1996).

Table 2 shows clearly that the RASS sample and the EMSS sample have the same distribution between the four studied spectral types. The EXOSAT sample has a different distribution. But the sample being rather small (28 late-type stars), the difference cannot be considered significant.

Figures 3 and 6 compare the cumulative X-ray luminosity function and the X-ray luminosities as a function of the distance from the Sun for our sample and the EMSS sample (Fleming 1988). For this we used the ROSAT data available for the EMSS sources (Fleming et al. 1995), allowing a direct comparison of the samples. For some of the EMSS sources, only an upper limit for f_X was given. These sources are given in Fig. 6 by downwards pointing arrows. Also shown in Fig. 6 is the curve of the X-ray luminosity as a function of distance, for a given flux f_X. This curve describes the effect of having stellar distances badly determined.

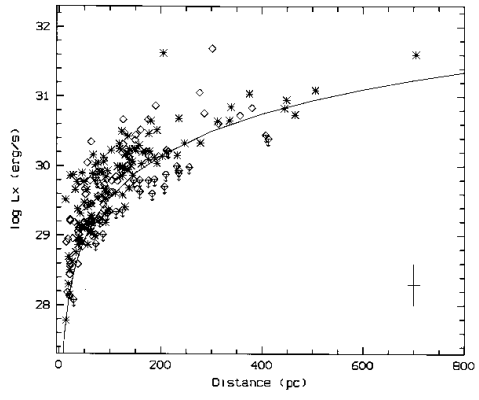

Fig. 6. X-ray luminosities as a function of distance for our RASS sample (∗) and for the EMSS sample (⋄) as taken from Fleming et al. (1995). The line drawn represents the X-ray luminosity as a function of distance for a constant observed flux $f_{\rm X}$

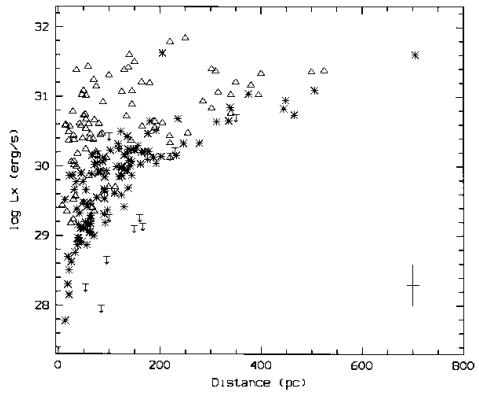

Fig. 7. X-ray luminosities as a function of distance for our RASS sample (∗) and for the sample of RS CVn stars (△) of Dempsey et al. (1993). For some of the RS CVn stars only upper limits for the X-ray luminosities were given. These objects are those indicated with the downwards pointing arrows

Both samples show a similar distribution of X-ray luminosities with distance, as well as similar X-ray luminosity functions. This leads to the conclusion that both samples come from the same population. This hypothesis was checked using a Kolmogorov-Smirnov test. The result was a disproof probability for the null hypothesis of $P = 2.5\%$, or a probability of both samples coming from the same population of 97.5%, which we take as a confirmation that indeed both samples are representative of the X-ray emitting solar-type population in the solar neighbourhood.

The major difference between the two samples is the high X-ray luminosity tail, composed of four stars with X-ray luminosities of the order 10^{32} erg s^{-1}, present in the EMSS sample. Out of these four stars one is a K giant, one a G subgiant, one a close binary (F8V + ?) and one a PMS star. All these sources are situated at more than 1000 pc from the Sun. Only two of them have been listed as observed by ROSAT: their ROSAT luminosity is also of the order of 10^{32} erg s^{-1}, and their PSPC countrates are well above the detection threshold of this survey. If such active stars were present in the study areas they were likely to be detected, but our sample does not contain such distant, extremely luminous sources. This difference could be due to slightly different spectral classification criteria adopted in the EMSS identification program and in the present work. Distinguishing between dwarfs and subgiants can be difficult, and a misclassification in luminosity class would lead to a huge difference in distance, and therefore in X-ray luminosity. In any case, these extremely active stars are very rare, as can be inferred by following the comparison with RS CVn systems.

Figure 7 shows a comparison of our sample of solar-type stars with the sample of RS CVn studied by Dempsey et al. (1993). For some of the RS CVn (marked with downwards pointing arrows), only an upper limit for the X-ray luminosity was given. Obvious is the greater spread in luminosity shown by the RS CVn sample. All our stars have similar X-ray luminosities as the low-luminosity RS CVn stars. So should our sample include RS CVn, those would only be at the low-activity end for this type of binaries. The reason for this could just be due to statistics, X-ray bright RS CVn not being all that numerous. Considering the number of objects in the sample of Dempsey et al. (1993), we should have ∼1.5 RS CVn in our sample, and ∼0.4 RS CVn if considering only the high-luminosity ones ($\log(L_{\rm X}) \geq 31$). Under such conditions, it is not so surprising that our sample does not contain any of the brightest RS CVn, and this suggests that the number of presently known very active, nearby RS CVn is probably not too underestimated.

3.4. A-type stars

The results of studies from previous X-ray observations, as well as the models used to explain the X-ray emission in stars, have led to the view that if X-ray emission was to be expected from A-stars, or more precisely, from single B7−A5 stars, it would be at only very weak levels of $\log(L_{\rm X}) \leq 10^{27}$ erg s^{-1} (see Golub et al. 1983). Exceptions to this rule are chemically peculiar Ap stars, and A-star binary systems, in which the X-ray emission is believed to come mainly from a later-type companion.

Our sample contains only one A-type star: RXJ 1446.3+0153 identified as 109 Vir, an A0V star. This star doesn't show photometric variability (see for example Lockwood & Thompson 1989). It doesn't display any peculiarity either, and is not known as a binary. It has been used as standard star in various studies. For instance as normal template A-star in a study of Ap stars (Gerbaldi et al. 1989) and as a spectrophotometric standard in the study of HH 46/47 (Raga & Mateo 1987). So far the most peculiar aspect of this star is

its high rotational velocity, found to be 340 km s^{-1} by Andrillat et al. (1995). Further studies of this object will be necessary to check out and confirm its identification as an X-ray source. With an L_X of $\sim 10^{28}$ erg s^{-1} the possibility of an X-ray coronal, low–mass companion cannot be excluded. Photometric studies (Lockwood & Thompson 1989) indicate that, if such a companion exists, it is much fainter than the A star, and not detectable with standard photometry. A search for radial velocity variations in the primary spectrum could be carried out, but the very high rotational velocity of the star makes the use of this technique very difficult.

4. Conclusions

We have presented an X-ray selected sample of solar-type stars observed by ROSAT in its all-sky survey. We have obtained the spectral classification from $BV(RI)_C$ observations, as well as the distances and X-ray luminosities. Most of the sample objects lie within a radius of 200 pc from the Sun. Apart from a few exceptions, they are all active stars. The X-ray luminosities are of the order of $10^{29} - 10^{30}$ erg s^{-1}, with a few objects having lower or higher luminosities. The hardness ratios are centered around a mean value of 0.13, quite typical for active stars.

A comparison with the Einstein EMSS sample shows that both samples have similar characteristics, and that they can therefore be considered as coming from the same population, representative of the solar-type X-ray population in the solar neighbourhood. The only difference between the samples is the presence of a high–luminosity tail (10^{32} erg s^{-1}) in the EMSS sample which is absent in our sample. Uncertainties in the determination of the stellar absolute magnitude could possibly be responsible for this difference, however, from the comparison with known RS CVn systems, we argue that very active A-K coronal sources are indeed rare.

The EXOSAT sample shows an apparently strong difference in the distribution in spectral types, but the low number of sources does not allow any statistical conclusions.

Our results allow us to determine at least some selection criteria for solar-type stellar sources in the RASS. The best candidates are sources with apparent visual magnitude brighter than 15mag and situated at less than $20''$ from the X-ray position. The sources should have a hardness ratio between -0.4 and 0.7, and a ratio of X-ray to visual flux included in the interval of $\log(f_X/f_V)$ from -5 to -1.8.

Acknowledgements. This research has made use of the SIMBAD database, operated at CDS, Strasbourg, France. The ROSAT project has been supported by the Bundesministerium für Forschung und Technologie (BMFT) and the Max-Planck-Gesellschaft (MPG). GC thank the European Southern Observatory for financial support, under the *"Senior Visitor Program"*, that made possible his permanence at ESO-Santiago

Appendix A
Sample information

Table 3 gives information about the ROSAT observation.

Column 1: the ROSAT name of the object, composed of the prefix RXJ and a short form of the coordinates.

Column 2: the coordinates of the X-ray source, as determined from the ROSAT plates (equinox 2000.0). The error for these positions is typically $30''$.

Column 3: the countrates for the X-ray sources, in counts per second.

Column 4: the total exposure time for each source.

Column 5: the hardness ratio 1 of each source.

Column 6: the coordinates, also for equinox 2000.0, of the stellar counterparts of the ROSAT sources.

Column 7: the distance between the X-ray position, as listed in Table 3 and the position of the counterpart, in arcseconds.

Column 8: the results from the spectral classification for the sample stars. For the binaries, the fact that the binarity/multiplicity obtained from the photometry was confirmed by the high-resolution spectra is indicated by a subscripted 1. A subscript 2 means the binarity was determined from the high-resolution spectra, a 3 means the binary is a visual one and a 4 means the binarity information was only obtained through the literature.

Column 9: the distance of the stars from the Sun, in pc, as determined using their $(B - V)$ colour index (see Sect. 2.4).

Column 10: the X-ray flux of the X-ray sources, in units of 10^{-12} erg s^{-1} cm^{-2}, as well as the errors for the flux.

Column 11: the X-ray luminosities of the studied stars, in units of 10^{29} erg s^{-1}, as well as the errors, as determined using the errors of the distance and X-ray flux.

Column 12: a catalogue name, whenever exiting.

Column 13: the spectral classification obtained either from the SIMBAD database or the low-resolution spectra taken in the course of the identification program.

Columns 14-17: the apparent visual magnitude and colours, in the $BV(RI)_C$ of the counterpart.

Appendix B
Notes on individual sources

RXJ 2331.4−4209: This object is a visual binary with a separation of $0''.4$, and a difference in magnitude of $\Delta m = 0.8$. The colour indices are consistent with two components of very near spectral types, in agreement with the small Δm.

Table 3. Summary of X-ray and observational data as well as results for the studied sample

ROSAT Name (1)	X-ray source coord. (2000.0)	Counts (3)	$t_{\rm Exp}$ (4)	HR 1 (5)	Counterpart coord. (2000.0)	Diff. (7)	Spect. Type (8)	Dist. (9)	f_X (10)	L_X (11)	Name (12)	Spo (13)	V (14)	B-V (15)	V-R (16)	V-I (17)
RXJ 2246.6−3928	22 46 33.4 −39 28 44	0.172	301.95	0.06	22 46 33.2 −39 28 45	2.5	G6V	66^{+04}_{-03}	$1.49^{+0.37}_{-0.33}$	$7.74^{+3.07}_{-2.26}$		G	9.45	0.71	0.40	0.77
RXJ 2258.3−4149	22 58 15.7 −41 49 47	0.107	121.32	0.57	22 58 16.5 −41 49 36	14.0	G6V+K1V[1]	136^{+13}_{-08}	$1.21^{+0.53}_{-0.48}$	$26.48^{+23.30}_{-13.46}$	CD-52 16149	K3	10.60	0.73	0.45	0.85
RXJ 2305.1−3823	23 05 03.4 −38 23 37	0.066	186.09	−0.23	23 05 04.5 −38 22 57	42.0	K1/3V	144 ± 10	$0.47^{+0.43}_{-0.30}$	$11.57^{+14.00}_{-08.00}$		K3	11.89	0.84	0.53	1.00
RXJ 2306.5−3855	23 06 32.5 −38 55 47	0.124	188.67	−0.03	23 06 34.4 −38 55 36	24.7	K4V	82 ± 3	$1.01^{+0.77}_{-0.58}$	$8.19^{+7.37}_{-4.94}$		K5	11.33	1.00	0.59	1.13
RXJ 2323.3−3730	23 23 15.4 −37 30 53	0.131	89.97	−0.12	23 23 14.2 −37 30 54	14.3	K1V	42 ± 2	$1.00^{+0.70}_{-0.52}$	$2.08^{+1.80}_{-1.17}$	HD 220345	K2III	9.35	0.87	0.47	0.89
RXJ 2331.4−4209	23 31 26.0 −42 09 43	0.153	147.09	0.38	23 31 25.7 −42 09 34	9.6	F9V+G1V[2,3]	77^{+6}_{-7}	$1.58^{+0.77}_{-0.62}$	$11.02^{+8.00}_{-5.50}$	HD 221330	G0V	8.25	0.58	0.34	0.64
RXJ 2356.2−3903	23 56 10.1 −39 03 05	0.089	114.97	−0.30	23 56 10.1 −39 03 05	15.0	K3V	21 ± 1	$0.60^{+0.58}_{-0.40}$	$0.32^{+0.35}_{-0.22}$	HD 224228	K3V	8.22	0.96	0.56	1.04
RXJ 0005.9−4145	00 05 52.2 −41 45 28	0.170	175.23	0.09	00 05 52.2 −41 45 08	20.0	G1V	37^{+3}_{-2}	$1.50^{+0.71}_{-0.44}$	$2.40^{+1.29}_{-0.85}$	HD 105	G0V	7.52	0.60	0.34	0.66
RXJ 0015.0−4036	00 14 59.8 −40 36 07	0.058	248.77	−0.18	00 14 57.4 −40 35 24	49.7	G4V	141^{+8}_{-6}	$0.42^{+0.38}_{-0.27}$	$10.10^{+11.38}_{-06.68}$		G5	10.74	0.65	0.36	0.70
RXJ 0022.2−3943	00 22 10.2 −39 43 25	0.037	332.04	0.13	00 22 10.6 −39 43 33	9.2	G3V+G5V[1]	336 ± 17	$0.33^{+0.27}_{-0.19}$	$44.56^{+44.60}_{-27.51}$		K3	11.96	0.67	0.39	0.78
RXJ 0027.7−4126	00 27 42.4 −41 26 07	0.215	297.42	0.28	00 27 42.7 −41 26 18	11.5	K4/5V	49^{+1}_{-2}	$2.11^{+1.56}_{-0.39}$	$5.97^{+4.97}_{-1.54}$		K5Ve	10.74	1.14	0.50	0.95
RXJ 0028.8−3930	00 28 50.4 −39 30 55	0.061	141.94	0.58	00 28 56.2 −39 30 50	67.3	K3/4V	92^{+4}_{-3}	$0.69^{+0.39}_{-0.31}$	$6.94^{+4.97}_{-3.36}$		K5V	10.61	1.01	0.56	1.04
RXJ 0032.1−3827	00 32 08.9 −38 27 17	0.049	363.41	0.42	00 32 09.9 −38 26 45	37.7	K3/4V	39^{+2}_{-1}	$0.52^{+0.32}_{-0.24}$	$0.92^{+0.72}_{-0.47}$		K5V	9.74	1.01	0.53	1.03
RXJ 0035.7−2513	00 35 43.7 −25 13 59	0.111	321.29	0.20	00 35 43.6 −25 14 03	4.2	G0V+G9V[1]	119^{+15}_{-08}	$1.04^{+0.63}_{-0.29}$	$17.55^{+11.86}_{-06.60}$	SAO 166391	G2V	9.70	0.63	0.37	0.71
RXJ 0038.6−2335	00 38 35.4 −23 35 46	0.042	331.72	0.03	00 38 36.2 −23 35 56	14.9	F3/4V	58 ± 3	$0.36^{+0.30}_{-0.21}$	$1.41^{+1.42}_{-0.89}$	HD 3581	F3IV/V	7.10	0.41	0.25	0.47
RXJ 0041.2−2649	00 41 10.8 −26 49 58	0.075	323.42	−0.22	00 41 11.5 −26 50 12	16.8	F9V+G8V[1]	124^{+09}_{-14}	$0.53^{+0.35}_{-0.27}$	$9.83^{+8.94}_{-5.95}$	HD 3877	G0V	9.86	0.60	0.37	0.71
RXJ 0042.7−2956	00 42 40.2 −29 56 49	0.037	342.35	0.60	00 42 40.3 −29 56 39	10.1	G3V	178^{+16}_{-13}	$0.43^{+0.23}_{-0.18}$	$16.13^{+13.30}_{-08.24}$		G5	11.18	0.64	0.34	0.69
RXJ 0045.0−4014	00 45 01.4 −40 14 31	0.033	369.93	−0.38	00 45 00.8 −40 14 31	6.7	K4/5V	125^{+12}_{-11}	$0.21^{+0.20}_{-0.13}$	$3.83^{+5.14}_{-2.72}$		dK8e	12.35	1.03	0.63	1.18
RXJ 0045.2−2455	00 45 09.1 −24 55 03	0.040	336.32	−0.40	00 45 06.4 −24 55 12	37.8	F6V+G2V[1]	192^{+21}_{-15}	$0.25^{+0.16}_{-0.12}$	$10.85^{+14.86}_{-07.55}$	HD 4288	F3/5V	9.89	0.46	0.34	0.65
RXJ 0047.3−2245	00 47 17.7 −22 45 02	0.196	355.23	0.09	00 47 17.8 −22 45 08	6.2	K4/5V	71^{+4}_{-3}	$1.72^{+0.37}_{-0.33}$	$10.47^{+3.87}_{-2.78}$		K8e	11.27	1.06	0.64	1.23
RXJ 0050.6−4221	00 50 34.5 −42 21 20	0.030	374.21	0.18	00 50 34.4 −42 21 17	3.2	F7/8V+G5V[1]	202^{+29}_{-20}	$0.28^{+0.23}_{-0.16}$	$13.75^{+18.60}_{-08.98}$	CD-43 234	F8	10.32	0.52	0.34	0.65
RXJ 0052.8−2728	00 52 45.4 −27 28 30	0.162	236.44	−0.25	00 52 45.6 −27 28 30	2.7	K5V	180^{+22}_{-20}	1.16 ± 0.35	$43.88^{+19.04}_{-19.08}$		K8V	12.34	1.10	0.70	1.38
RXJ 0053.0−3021	00 52 59.1 −30 21 33	0.051	331.67	−0.56	00 52 59.8 −30 21 24	12.8	K2/3V	14	$0.27^{+0.19}_{-0.14}$	$0.06^{+0.05}_{-0.03}$	HD 5133	K3V+..	7.17	0.93	0.54	1.01
RXJ 0055.5−3731	00 55 28.8 −37 31 40	0.044	360.75	−0.22	00 55 26.5 −37 31 24	31.7	G6V	46^{+3}_{-2}	$0.32^{+0.28}_{-0.20}$	$0.80^{+0.88}_{-0.53}$	HD 5403	G5V	8.67	0.71	0.41	0.77
RXJ 0100.2−3818	01 00 13.3 −38 18 36	0.128	389.43	0.37	01 00 12.3 −38 18 38	11.9	K4V	54 ± 3	$1.32^{+0.31}_{-0.28}$	$4.53^{+1.28}_{-1.21}$		K5Ve	10.58	1.04	0.61	1.15
RXJ 0105.4−4016	01 05 21.9 −40 16 09	0.032	427.35	−0.11	01 05 21.7 −40 16 11	3.0	F3V	62^{+3}_{-5}	$0.25^{+0.22}_{-0.15}$	$1.14^{+1.21}_{-0.78}$	HD 6493	F3V	7.17	0.40	0.24	0.46
RXJ 0116.8−3932	01 16 49.4 −39 32 10	0.024	404.78	0.51	01 16 50.6 −39 32 07	14.2	K1V	21 ± 1	$0.27^{+0.17}_{-0.13}$	$0.14^{+0.11}_{-0.07}$	HD 7777	G8	7.97	0.89	0.47	0.90
RXJ 0121.2−3729	01 21 10.0 −37 29 28	0.386	370.78	0.03	01 21 10.0 −37 29 29	1.0	K5V	45^{+3}_{-2}	$3.27^{+0.47}_{-0.44}$	$7.92^{+2.49}_{-1.67}$		K8e	10.52	1.12	0.71	1.38
RXJ 0121.5−4058	01 21 29.6 −40 58 17	0.058	420.78	−0.03	01 21 29.3 −40 58 17	3.4	F6V[3,4]	90^{+9}_{-8}	$0.47^{+0.19}_{-0.16}$	$4.62^{+3.19}_{-2.07}$	HD 8283	F3V	8.58	0.48	0.29	0.55
RXJ 0125.6−4148	01 25 33.7 −41 48 35	0.076	406.44	0.20	01 25 33.6 −41 48 36	1.5	G5V+K3V[1]	130^{+08}_{-11}	$0.71^{+0.24}_{-0.21}$	$14.38^{+7.34}_{-5.91}$	VW Phe	G2	10.48	0.72	0.47	0.89
RXJ 0126.4−4127	01 26 25.3 −41 27 54	0.037	426.96	0.66	01 26 25.3 −41 27 49	5.0	G8V	91^{+7}_{-8}	$0.44^{+0.21}_{-0.17}$	$4.33^{+3.00}_{-2.11}$		K0V	10.30	0.74	0.42	0.78
RXJ 0135.8−3956	01 35 48.5 −39 56 44	0.056	363.04	0.03	01 35 49.3 −39 56 30	16.7	F4V	40^{+2}_{-4}	$0.48^{+0.36}_{-0.27}$	$0.91^{+0.85}_{-0.58}$	HD 9895	F3/5V	6.41	0.43	0.25	0.48
RXJ 0136.8−3811	01 36 47.6 −38 11 19	0.072	193.69	0.46	01 36 48.4 −38 11 26	11.7	K2/3V	137^{+15}_{-10}	$0.77^{+0.48}_{-0.36}$	$17.43^{+17.43}_{-09.53}$		K0V	12.12	0.91	0.54	1.03
RXJ 0141.4−3808	01 41 25.5 −38 08 06	0.096	424.82	−0.04	01 41 28.6 −38 08 23	40.3	F3V	39^{+2}_{-3}	$0.78^{+0.24}_{-0.21}$	$1.44^{+0.63}_{-0.56}$	HD 10481	F2V	6.18	0.41	0.24	0.45

Table 3. continued

ROSAT Name (1)	X-ray source coord. (2000.0)	Counts (3)	$t_{\rm Exp}$ (4)	HR 1 (5)	Counterpart coord. (2000.0)	Diff. (7)	Spect. Type (8)	Dist. (9)	f_X (10)	L_X (11)	Name (12)	Spo (13)	V (14)	B-V (15)	V-R (16)	V-I (17)
RXJ 0155.4−3846	01 55 21.5 −38 46 22	0.470	260.55	−0.48	01 55 22.5 −38 46 23	11.7	K5V	67±4	$2.71^{+0.57}_{-0.52}$	$14.35^{+5.23}_{-3.96}$		K5V	11.15	1.07	0.70	1.36
RXJ 0440.3−5856	04 40 17.2 −58 56 31	0.160	81.89	−1.05	04 40 17.6 −58 56 43	12.4	G5V	19±1	$0.44^{+0.68}_{-0.44}$	$0.20^{+0.34}_{-0.19}$	HD 30003	G5V	6.53	0.68	0.38	0.72
RXJ 0450.1−5856	04 50 07.4 −58 56 52	0.933	14.69	...	04 50 09.7 −58 57 31	42.9	K2V	205^{+20}_{-30}	$8.40^{+5.40}_{-4.00}$	$421.08^{+244.26}_{-199.66}$	HD 31746	K2	12.91	0.89	0.50	0.99
RXJ 0454.9−5832	04 54 53.0 −58 32 54	0.470	93.74	−0.04	04 54 53.1 −58 32 54	0.8	F5V	32^{+3}_{-1}	$3.81^{+2.01}_{-1.63}$	$4.58^{+3.83}_{-2.19}$		F3V	6.11	0.44	0.27	0.52
RXJ 0501.5−5930	05 01 31.8 −59 30 51	0.024	545.99	...	05 01 32.3 −59 30 46	6.3	F9V+G6V[1]	232^{+21}_{-24}	$0.22^{+0.13}_{-0.12}$	$14.14^{+13.08}_{-09.00}$		G2V	10.85	0.58	0.35	0.67
RXJ 0505.5−5728	05 05 30.8 −57 28 15	2.024	131.23	−0.02	05 05 31.1 −57 28 25	11.5	F7/8V	13±1	$15.64^{+1.94}_{-1.66}$	$3.28^{+0.92}_{-0.74}$	HD 33262	F7V	4.70	0.52	0.31	0.60
RXJ 0505.6−5755	05 05 33.9 −57 55 28	0.158	405.21	0.17	05 05 36.4 −57 55 36	21.4	K4V	87^{+5}_{-7}	$1.46^{+0.33}_{-0.30}$	$13.30^{+5.11}_{-4.27}$		K8	11.41	0.99	0.61	1.19
RXJ 0505.8−6210	05 05 47.5 −62 10 10	0.063	367.77	0.43	05 05 47.3 −62 09 58	12.1	K5V	157^{+21}_{-20}	$0.67^{+0.34}_{-0.28}$	$19.66^{+18.40}_{-14.60}$		K8	13.28	1.14	0.64	1.25
RXJ 0507.6−5459	05 07 33.3 −54 59 04	0.047	269.80	...	05 07 34.3 −54 59 21	19.1	F5/6V	50^{+5}_{-4}	$0.42^{+0.26}_{-0.22}$	$1.26^{+0.76}_{-0.76}$	HD 33514	F5V	7.34	0.47	0.28	0.54
RXJ 0508.1−5316	05 08 04.2 −53 16 20	0.072	137.11	0.05	05 08 07.0 −53 16 15	25.6	G3V	150^{+13}_{-11}	$0.62^{+0.48}_{-0.34}$	$16.65^{+18.05}_{-10.23}$		G6V	10.81	0.64	0.37	0.68
RXJ 0510.4−5732	05 10 26.2 −57 32 30	0.047	577.76	−0.40	05 10 26.8 −57 31 59	31.4	F9V+G5V[1]	247^{+27}_{-23}	$0.29^{+0.21}_{-0.16}$	$21.19^{+21.32}_{-13.74}$		G2V	10.93	0.57	0.34	0.67
RXJ 0513.2−5507	05 13 11.5 −55 07 44	0.075	158.43	0.44	05 13 12.0 −55 07 48	5.9	K5/7V	95^{+12}_{-14}	$0.79^{+0.52}_{-0.39}$	$8.54^{+9.32}_{-5.40}$		K8V	12.54	1.22	0.77	1.51
RXJ 0516.1−6006	05 16 07.2 −60 06 14	0.136	130.19	0.29	05 16 04.7 −60 06 55	45.0	K4/5V	102^{+10}_{-9}	$1.34^{+0.76}_{-0.59}$	$16.76^{+14.74}_{-09.15}$		K5	12.12	1.08	0.63	1.19
RXJ 0518.7−5803	05 18 43.3 −58 03 11	0.053	129.22	1.00	05 18 42.4 −58 02 48	25.0	K4V	236^{+31}_{-28}	$0.72^{+0.47}_{-0.36}$	$47.84^{+53.43}_{-29.29}$		K5	13.66	1.01	0.62	1.10
RXJ 0519.2−5756	05 19 14.3 −57 56 59	0.023	567.70	...	05 19 16.4 −57 56 53	16.2	G5V+K3V[1]	466^{+29}_{-56}	$0.21^{+0.13}_{-0.11}$	$54.24^{+44.16}_{-34.50}$		G5V	13.25	0.71	0.43	0.87
RXJ 0523.2−5751	05 23 15.4 −57 51 14	0.088	227.92	−0.09	05 23 15.3 −57 51 01	13.0	K1/2V	136^{+13}_{-12}	$0.69^{+0.28}_{-0.23}$	$15.14^{+10.30}_{-06.81}$		G	11.81	0.85	0.52	1.02
RXJ 0523.7−6041	05 23 41.4 −60 41 31	0.050	388.88	0.37	05 23 43.2 −60 41 25	14.5	K5/7V	125^{+19}_{-12}	$0.51^{+0.22}_{-0.18}$	$9.48^{+8.11}_{-5.14}$		K5	12.98	1.19	0.67	1.33
RXJ 0525.8−5451	05 25 47.5 −54 51 11	0.019	830.29	−0.31	05 25 46.6 −54 51 21	12.7	K3V	129^{+14}_{-13}	$0.13^{+0.10}_{-0.07}$	$2.58^{+2.93}_{-1.63}$		K5	12.13	0.95	0.54	1.04
RXJ 0527.6−6024	05 27 39.1 −60 24 53	0.172	147.20	−0.32	05 27 40.3 −60 24 53	8.9	G9V	18±1	$1.14^{+0.46}_{-0.38}$	$0.45^{+0.19}_{-0.24}$	HD 36435	G6V	7.01	0.77	0.41	0.80
RXJ 0528.3−6052	05 28 20.2 −60 52 03	0.045	463.20	...	05 28 21.9 −60 51 59	13.0	F5V	136^{+16}_{-13}	$0.40^{+0.24}_{-0.20}$	$8.75^{+8.11}_{-4.68}$	HD 36530	F3V	9.53	0.44	0.27	0.57
RXJ 0531.8−5239	05 31 50.3 −52 39 52	0.03453	212.87	−0.40	05 31 51.3 −52 40 00	9.3	K4V	137^{+17}_{-16}	$0.21^{+0.23}_{-0.15}$	$4.81^{+7.78}_{-3.64}$		K8V	12.52	1.02	0.59	1.13
RXJ 0534.4−6006	05 34 24.6 −60 06 24	0.08246	123.17	−0.39	05 34 26.3 −60 06 15	15.6	F7V	76^{+7}_{-5}	$0.51^{+0.42}_{-0.29}$	$3.53^{+4.18}_{-2.21}$	HD 37402	F8	8.40	0.50	0.30	0.58
RXJ 0535.0−6110	05 34 57.5 −61 10 36	0.04966	181.42	0.51	05 34 57.6 −61 10 32	4.1	G8/9IV	44	$0.55^{+0.32}_{-0.25}$	$1.28^{+0.74}_{-0.59}$	HD 37501	G5IV	6.33	0.84	0.45	0.88
RXJ 0538.2−5555	05 38 13.2 −55 55 55	0.01968	231.25	0.66	05 38 08.6 −55 56 02	39.3	K3V	278^{+37}_{-31}	$0.23^{+0.17}_{-0.13}$	$21.39^{+26.06}_{-14.08}$		K7V	13.79	0.95	0.49	1.06
RXJ 0538.4−5718	05 38 24.5 −57 18 57	0.07249	214.93	−0.19	05 38 24.6 −57 19 08	11.0	F9V	139^{+10}_{-09}	$0.53^{+0.42}_{-0.30}$	$12.131^{+12.73}_{-07.80}$		G	10.06	0.55	0.33	0.63
RXJ 0539.1−5657	05 39 05.4 −56 57 54	0.03230	211.54	0.09	05 39 05.2 −56 57 58	4.3	K1/2V	445^{+58}_{-54}	$0.28^{+0.24}_{-0.17}$	$66.93^{+102.89}_{-045.62}$		K2V	14.49	0.87	0.52	0.97
RXJ 0540.0−5343	05 40 01.4 −53 43 42	0.04626	216.42	0.44	05 39 59.3 −53 43 43	18.6	K0V	164^{+24}_{-18}	$0.49^{+0.34}_{-0.25}$	$15.71^{+19.30}_{-09.60}$		G2V	11.97	0.80	0.44	0.86
RXJ 0541.1−6151	05 41 04.4 −61 51 23	0.07700	116.21	0.24	05 41 04.9 −61 51 29	7.0	F3/4V	192^{+19}_{-17}	$0.74^{+0.52}_{-0.38}$	$32.51^{+34.34}_{-19.57}$	HD 38372	F0V	9.62	0.38	0.27	0.50
RXJ 0543.9−6005	05 43 51.7 −60 05 56	0.11020	166.24	−0.22	05 43 49.7 −60 05 54	15.1	G7V+K2V[1]	176^{+12}_{-11}	$0.79^{+0.55}_{-0.41}$	$29.12^{+27.18}_{-17.04}$		G6	11.31	0.74	0.44	0.91
RXJ 0544.4−5523	05 44 21.1 −55 23 36	0.03298	246.20	0.55	05 44 20.7 −55 23 30	6.9	K5/7V	63^{+8}_{-9}	$0.37^{+0.22}_{-0.17}$	$1.76^{+1.81}_{-1.08}$		K5	11.70	1.23	0.68	1.26
RXJ 0545.3−5543	05 45 15.2 −55 43 22	0.02054	1328.46	−0.18	05 45 14.9 −55 43 27	5.6	F5V+G6V[1]	92^{+8}_{-13}	$0.15^{+0.09}_{-0.07}$	$1.52^{+1.41}_{-0.86}$	HD 38829	F5V	8.22	0.49	0.29	0.54
RXJ 0545.4−5411	05 45 26.9 −54 11 48	0.06019	273.92	−0.14	05 45 26.8 −54 11 34	14.0	K3V+K4V[3]	129^{+13}_{-47}	$0.45^{+0.32}_{-0.24}$	$9.01^{+9.56}_{-7.26}$		K5+K8	11.51	0.98	0.61	1.12
RXJ 0547.3−5450	05 47 17.8 −54 50 35	0.02892	377.36	−0.20	05 47 17.9 −54 50 28	7.0	F6V	90^{+24}_{-8}	$0.21^{+0.20}_{-0.14}$	$2.02^{+2.30}_{-1.44}$	HD 39139	F6V	8.77	0.49	0.28	0.57
RXJ 0548.0−6241	05 48 01.0 −62 41 14	0.04201	205.78	0.53	05 48 02.3 −62 41 08	10.8	K0/1V	170^{+24}_{-22}	$0.47^{+0.31}_{-0.25}$	$16.05^{+20.53}_{-09.98}$		G6V	12.00	0.79	0.47	0.92

Table 3. continued

ROSAT Name (1)	X-ray source coord. (2000.0)	Counts (3)	t_{Exp} (4)	HR 1 (5)	Counterpart coord. (2000.0)	Diff. (7)	Spect. Type (8)	Dist. (9)	f_X (10)	L_X (11)	Name (12)	Sp$_0$ (13)	V (14)	B-V (15)	V-R (16)	V-I (17)
RXJ 0549.7−5950	05 49 42.1 −59 50 10	0.07317	334.29	0.17	05 49 41.1 −59 50 23	15.0	F7/8V[2,3]	148^{+67}_{-13}	$0.67^{+0.37}_{-0.29}$	$17.57^{+12.24}_{-09.26}$	HD 39579	F7V	8.86	0.53	0.29	0.55
RXJ 1053.9−2423	10 53 51.1 −24 23 25	0.03141	365.48	0.46	10 53 53.0 −24 23 35	27.8	K4V	175^{+78}_{-23}	$0.34^{+0.17}_{-0.12}$	$12.37^{+8.59}_{-04.59}$		K2/5V	13.17	1.05	0.60	1.16
RXJ 1056.1−2653	10 56 04.7 −26 53 13	0.04892	376.16	0.00	10 56 02.4 −26 52 47	40.3	G5V	120^{+10}_{-11}	$0.41^{+0.32}_{-0.23}$	$6.94^{+7.59}_{-4.51}$		G8V+K8V	10.48	0.67	0.38	0.74
RXJ 1058.2−2926	10 58 11.6 −29 26 29	0.07483	314.47	0.01	10 58 14.1 −29 26 12	36.8	K0V+K5V[1]	115^{+20}_{-17}	$0.62^{+0.38}_{-0.29}$	$9.83^{+11.92}_{-6.04}$		G5V	10.98	0.82	0.50	1.02
RXJ 1101.1−3132	11 01 10.1 −31 32 48	0.08260	374.20	−0.02	11 01 10.9 −31 32 49	10.3	K3V	57^{+3}_{-3}	$0.68^{+0.22}_{-0.20}$	$2.60^{+1.20}_{-0.92}$		K7V	10.30	0.94	0.55	1.10
RXJ 1102.1−2252	11 02 07.2 −22 52 37	0.03021	379.49	−0.37	11 02 06.7 −22 52 33	8.0	K7V	57^{+8}_{-7}	$0.19^{+0.18}_{-0.13}$	$0.74^{+1.16}_{-0.54}$	1E 1059.6-2236	K5Ve	11.77	1.28	0.80	1.55
RXJ 1108.5−3007	11 08 35.0 −30 07 41	0.01492	368.85	0.55	11 08 34.4 −30 07 39	8.0	F5/6V	70±3	$0.17^{+0.09}_{-0.07}$	$0.99^{+0.92}_{-0.59}$	HD 96803	F5V	7.94	0.46	0.29	0.58
RXJ 1110.5−3027	11 10 35.7 −30 27 20	0.02981	352.19	0.61	11 10 34.1 −30 27 16	21.1	F3V+F7V[1]	161^{+16}_{-14}	$0.34^{+0.17}_{-0.14}$	$10.68^{+8.65}_{-5.47}$	HD 97131	F2V	8.81	0.41	0.26	0.53
RXJ 1110.6−2853	11 10 39.8 −28 53 34	0.04913	356.77	0.39	11 10 38.0 −28 54 01	35.9	F4V	339^{+33}_{-30}	$0.51^{+0.31}_{-0.24}$	$69.74^{+63.94}_{-34.13}$		F2V	11.05	0.42	0.26	0.51
RXJ 1115.9−2750	11 15 54.8 −27 50 19	0.03979	176.42	0.47	11 15 55.9 −27 50 15	15.1	K5V	50±3	$0.43^{+0.28}_{-0.22}$	$1.27^{+1.12}_{-0.71}$		K5V	10.92	1.17	0.64	1.22
RXJ 1118.3−3234	11 18 23.8 −32 34 48	0.03091	345.01	0.68	11 18 23.1 −32 34 23	26.5	K2/3V	449^{+78}_{-62}	$0.37^{+0.28}_{-0.18}$	$88.36^{+126.37}_{-069.07}$		K0V	14.56	0.88	0.59	1.03
RXJ 1119.5−2351	11 19 29.4 −23 51 49	0.02572	333.33	0.60	11 19 30.1 −23 52 02	16.2	K1V	145^{+16}_{-15}	$0.29^{+0.18}_{-0.14}$	$7.36^{+4.27}_{-3.03}$		G4V	12.00	0.86	0.46	0.92
RXJ 1121.5−3131	11 21 34.6 −31 31 40	0.05148	339.31	0.09	11 21 35.4 −31 31 16	26.1	F7/8V	54^{+3}_{-2}	$0.45^{+0.34}_{-0.22}$	$1.55^{+1.45}_{-0.77}$	HD 98753	F6V	7.74	0.51	0.30	0.60
RXJ 1121.8−2411	11 21 49.1 −24 11 16	0.06001	349.36	0.23	11 21 49.8 −24 11 23	11.9	G3V	43^{+3}_{-3}	$0.57^{+0.32}_{-0.25}$	$1.29^{+0.63}_{-0.51}$	HD 98764	G5	8.12	0.64	0.37	0.74
RXJ 1122.0−2446	11 22 04.6 −24 46 34	0.97300	190.91	0.02	11 22 05.4 −24 46 38	11.6	K4/5V+...[1,4]	28^{+4}_{-9}	$8.19^{+0.99}_{-0.94}$	$7.40^{+3.23}_{-4.35}$	HD 98800	K5V + ??	8.94	1.26	0.80	1.59
RXJ 1122.9−2545	11 22 55.9 −25 45 39	0.05560	329.36	−0.22	11 22 56.0 −25 45 53	14.1	K4/5V	64^{+5}_{-4}	$0.40^{+0.28}_{-0.21}$	$1.92^{+1.89}_{-1.12}$		K8Ve	11.24	1.11	0.63	1.16
RXJ 1123.3−2342	11 23 18.1 −23 42 27	0.03630	354.64	0.09	11 23 18.4 −23 42 25	4.6	G8III	187±4	$0.31^{+0.26}_{-0.19}$	$13.30^{+12.02}_{-08.00}$	HD 98975	K0	7.17	0.94	0.50	0.97
RXJ 1124.0−2404	11 24 02.5 −24 04 34	0.06691	170.75	0.35	11 24 00.4 −24 04 44	30.4	F8V+G4V[1]	705^{+50}_{-56}	$0.68^{+0.41}_{-0.32}$	$402.43^{+340.96}_{-219.66}$		F8V	13.03	0.54	0.34	0.66
RXJ 1132.9−3151	11 32 58.0 −31 51 42	0.42410	140.08	0.20	11 33 00.4 −31 51 10	44.2	G8III	35±1	$3.97^{+0.90}_{-0.71}$	$5.91^{+4.41}_{-2.71}$	HD 100407	G7III	3.54	0.94	0.33	0.68
RXJ 1345.2−0043	13 45 10.3 −00 43 39	0.03977	412.91	0.21	13 45 10.3 −00 43 58	19.0	F8V	312^{+30}_{-27}	$0.37^{+0.27}_{-0.20}$	$43.43^{+46.38}_{-26.66}$		F8V	11.67	0.39	0.32	0.62
RXJ 1354.2−0157	13 54 09.0 −01 57 03	0.03931	386.38	−0.08	13 54 07.3 −01 57 56	58.8	F8V	64^{+5}_{-5}	$0.31^{+0.19}_{-0.16}$	$1.50^{+1.08}_{-0.68}$	HD 121218	F8	8.32	0.54	0.31	0.62
RXJ 1354.9−0222	13 54 51.8 −02 22 53	0.02611	395.91	−0.06	13 54 51.9 −02 22 50	3.3	F9V+G5V[1]	97^{+08}_{-11}	$0.21^{+0.19}_{-0.13}$	$2.33^{+2.94}_{-1.65}$	HD 121322	F8V	8.89	0.56	0.34	0.67
RXJ 1355.5+0015	13 55 27.5 +00 15 26	0.02540	378.16	0.23	13 55 27.8 +00 15 23	5.4	K5/7V	62^{+9}_{-5}	$0.24^{+0.20}_{-0.14}$	$1.10^{+1.52}_{-0.71}$		K8	11.95	1.28	0.73	1.40
RXJ 1358.4−0139	13 58 24.9 −01 39 45	0.16000	415.62	0.48	13 58 24.8 −01 39 38	7.1	G0V+G5V[1]	123^{+14}_{-07}	$1.74^{+0.35}_{-0.32}$	$31.32^{+15.54}_{-08.60}$	HD 121909	G0	9.61	0.61	0.35	0.71
RXJ 1358.9+0058	13 58 52.1 +00 58 00	0.03765	412.89	0.39	13 58 52.2 +00 58 00	1.5	G9V+G9V[1]	125^{+09}_{-16}	$0.39^{+0.25}_{-0.19}$	$7.24^{+6.38}_{-3.40}$	BD+01 2868	G5V	10.38	0.76	0.43	0.84
RXJ 1401.9+0025	14 01 53.4 +00 25 14	0.06633	424.22	0.15	14 01 52.1 +00 25 20	20.4	F8V	63^{+5}_{-3}	$0.60^{+0.26}_{-0.26}$	$2.86^{+1.37}_{-1.21}$	HD 122444	F8V	8.30	0.54	0.30	0.58
RXJ 1404.0−0021	14 04 02.4 −00 21 41	0.09041	433.98	0.71	14 04 02.2 −00 21 45	5.8	F9V+G5V[1]	79^{+7}_{-9}	$1.09^{+0.31}_{-0.27}$	$8.21^{+4.26}_{-3.33}$	HD 122798	F8V	8.50	0.58	0.34	0.67
RXJ 1411.5+0121	14 11 31.7 +01 21 59	0.07068	460.05	−0.41	14 11 31.2 +01 21 44	16.8	F6V	33±3	$0.43^{+0.28}_{-0.21}$	$0.57^{+0.54}_{-0.33}$	HD 124115	F7V	6.41	0.48	0.28	0.55
RXJ 1413.7−0050	14 13 40.5 −00 50 45	0.11520	407.59	0.08	14 13 40.6 −00 05 40	5.2	F6V	50^{+33}_{-14}	$1.01^{+0.30}_{-0.26}$	$3.02^{+7.78}_{-1.88}$	HD 124425	F7V	5.90	0.47	0.28	0.55
RXJ 1428.2−0213	14 28 12.3 −02 13 40	1.34100	348.03	0.16	14 28 12.1 −02 13 36	5.0	G6IV+K5V[4]	22	$12.49^{+0.75}_{-0.44}$	$7.28^{+0.62}_{-0.60}$	HD 126868	G2IV+G4V	4.82	0.74	0.39	0.75
RXJ 1429.4−0049	14 29 26.1 −00 49 34	0.12030	356.67	0.41	14 29 26.2 −00 49 46	12.1	K0V	87±6	$1.26^{+0.32}_{-0.30}$	$11.50^{+5.66}_{-3.88}$	BD-00 2832	G5V	10.66	0.81	0.47	0.82
RXJ 1432.1−0114	14 32 07.5 −01 14 42	0.04044	338.43	0.05	14 32 07.4 −01 14 47	5.2	K3/4V[2,4]	91^{+9}_{-8}	$0.35^{+0.29}_{-0.20}$	$3.40^{+4.08}_{-1.95}$	CM Vir	G2/5V	11.62	1.02	0.56	1.04
RXJ 1433.3−0126	14 33 20.5 −01 26 43	0.03981	323.97	0.34	14 33 20.5 −01 25 44	1.0	K0/1V	506^{+16}_{-075}	$0.40^{+0.30}_{-0.21}$	$122.72^{+192.24}_{-079.43}$		K5	14.32	0.78	0.50	0.92
RXJ 1436.9−0239	14 36 52.1 −02 44 19	0.02660	342.78	0.41	14 36 54.2 −02 44 32	34.0	K4/5V	111±12	$0.28^{+0.19}_{-0.14}$	$4.07^{+4.41}_{-2.49}$		K5	12.32	1.09	0.61	1.19

ROSAT Name (1)	X-ray source coord. (2000.0)	Counts (3)	t_{Exp} (4)	HR 1 (5)	Counterpart coord. (2000.0)	Diff. (7)	Spect. Type (8)	Dist. (9)	f_X (10)	L_X (11)	Name (12)	Sp$_0$ (13)	V (14)	B-V (15)	V-R (16)	V-I (17)
RXJ 1437.5+0216	14 37 29.3 +02 16 48	0.04645	341.86	0.60	14 37 29.3 +02 16 40	8.0	F9V[3,4]	26^{+1}_{-2}	$0.53^{+0.23}_{-0.19}$	$0.42^{+0.24}_{-0.19}$	HD 128563	F8	6.45	0.56	0.32	0.62
RXJ 1442.7−0039	14 42 44.2 −00 39 57	0.12920	352.06	0.25	14 42 44.3 −00 39 54	3.3	G5V+K1V[1]	118^{+28}_{-10}	$1.24^{+0.46}_{-0.36}$	$20.66^{+13.78}_{-10.89}$		K5	10.12	0.70	0.41	0.82
RXJ 1446.3+0153	14 46 15.9 +01 53 43	0.05266	356.60	−0.03	14 46 14.7 +01 53 13	26.9	A0V	41^{+4}_{-6}	$0.43^{+0.28}_{-0.21}$	$0.73^{+0.71}_{-0.42}$	HD 130109	A0V	3.72	−0.01		
RXJ 1450.7+0055	14 50 39.8 +00 55 46	0.05165	300.38	0.81	14 50 38.2 +00 55 53	25.0	F6V	375^{+36}_{-33}	$0.65^{+0.23}_{-0.20}$	$109.05^{+67.79}_{-46.49}$		F	11.67	0.48	0.29	0.58
RXJ 1451.9+0201	14 51 52.1 +02 01 05	0.05675	359.47	−0.18	14 51 53.3 +02 00 51	22.8	G5/6V	41^{+3}_{-2}	$0.42^{+0.34}_{-0.25}$	$0.83^{+0.87}_{-0.53}$	HD 131179	G5V	8.34	0.70	0.39	0.75

RXJ 0053.0−3021: HD 5133. The $(B-V)$ index yields a distance of 12 pc for this object, which is in good accordance with the distance of 13 pc given by the trigonometric parallax ($\pi = 0\farcs075$, Hipparcos Input Catalogue).

RXJ 0121.5−4058: This is also a visual binary, with a separation of $6\farcs1$, and a Δm of 5.5. Only one component is therefore detectable in the photometry, the other being too faint.

RXJ 0440.3−5856: It has a very soft X-ray spectrum, and a rather low X-ray luminosity. This is an X-ray quiet object, detected only due to its nearness to the Sun (∼19 pc, or 17 pc according to the measured trigonometric parallax ($\pi = 0\farcs059$, Hipparcos Input Catalogue)).

RXJ 0505.6−5728: $V = 4.7$. This star was not observed, as it is too bright for the photomultiplier tubes. The colours and spectral classification were taken from the literature (Bessel 1990). The distance determined using those colours agrees very well with the distance derived from the trigonometric parallax (13 pc, $\pi = 0\farcs078$).

RXJ 0527.6−6024: this star has a measured trigonometric parallax that gives a distance of 25 pc ($\pi = 0\farcs040 \pm 0\farcs013$, Hipparcos Input Catalogue). The value found using the colour index $(B-V)$ is quite smaller (19 pc), but still within the error box of the distance given by the trigonometric parallax.

RXJ 0545.3−5543: this is another visual binary with a separation of $7\farcs5$ and a difference in visual magnitude of $\Delta m = 1.8$. The photometric colours measured agree well with a binary.

RXJ 0549.7−5950: the photometric colours correspond to a F7/8V star, but the object is a visual binary with a separation of $2\farcs5$ and a difference in visual magnitude of $\Delta m = 0.4$. The spectroscopic observation available shows the system to be actually triple. From the similarity between the three spectroscopic components and the value of Δm we assume the three components to be of very similar spectral types, and the brighter of the two visual objects to be a binary. For the distance determination, a combination of three F7/8 stars was used.

RXJ 1122.0−2446: the photometric colours give K5/7V as spectral classification. The object is a known visual binary with a separation of $0\farcs2$ and a difference in visual magnitude of $\Delta m = 0.3$, in which both visual components are binaries as well. The spectral types are (see Soderblom et al. 1996): component A: K4-5V + ??, component B: K7V + M1V. We used these spectral types to infer the distance.

RXJ 1132.9−3151: the visual magnitude being of $V = 3.54$, this object also has photometry taken from the literature (Eggen 1977). As no Cousin's $(V-R)_C$ and $(V-I)_C$ colours could be found in the literature, the given indices are in the Johnson system. The distance infered from the $(B-V)$ colour lies just in the limit, but still within the error box of the distance given by the trigonometric parallax of this star (53 pc, $\pi = 0\farcs019 \pm 0\farcs010$, Hipparcos Input Catalogue).

RXJ 1413.7−0050: the trigonometric parallax of this star gives a distance of 50 pc, with a range of 36 pc to 83 pc ($\pi = 0\farcs020 \pm 0\farcs008$, Hipparcos Input Catalogue). This star is classified as an F7Vw, so it can't be treated as a normal main-sequence star. We have therefore adopted the distance given by the trigonometric parallax to calculate its X-ray luminosity.

RXJ 1428.2−0213: with a visual magnitude of $V = 4.89$, this object was also too bright to be observed with the 50 cm ESO. The values for the photometric colours were taken from literature (Bessel 1990). The values of the colours, as well as the measured difference in visual magnitude ($\Delta m = 4.2$) between the two components do not agree very well with the spectral classification given in the literature (G2IV+G4V), but rather with our spectral types G6IV+K5V. The distance infered using our spectral classification (22 pc) agrees very well with the distance of 23 pc given by the trigonometric parallax ($\pi = 0''.43$, Hipparcos Input Catalogue).

RXJ 1437.5+0216: another visual binary. The separation is of $1\farcs9$, and the difference in visual magnitude of $\Delta m = 4.0$.

RXJ 1446.3+0153: $V = 3.72$. A0/1V star. It is not very clear yet whether this is really the source of the X-ray emission ($\log(L_X) = 28.9$) (see Sect. 3.4). The trigonometric parallax ($\pi = 0\farcs030 \pm 0\farcs050$, Hipparcos Input Catalogue) gives a distance of 33 pc, in reasonable agreement with the one calculated with the colour index.

References

Andrillat Y., Jaschek C., Jaschek M., 1995, A&AS 112, 475

Bessel M.S., 1990, A&AS 83, 357

Cruddace R.G., Hasinger G., Trümper J., Schmitt J.H.M.M., Hartner G.D., 1991, Exper. Astron. 1, 365

Cutispoto G., Tagliaferri G., Pallavicini R., Pasquini L., Rodono M., 1996, A&AS 115, 41

Danziger I.J., et al., 1990, ESO Messenger 62, 4

Dempsey R.C., Linsky J.L., Fleming T.A., Schmitt J.H.M.M., 1993, ApJS 86, 599

Eggen O.J., 1977, ApJ 215, 812

Fleming T.A., 1988, Ph.D. dissertation, University of Arizona

Fleming T.A., Gioia I.M., Maccacaro T., 1989, ApJ 340, 1011

Fleming T.A., Molendi S., Maccacaro T., Wolter A., 1995, ApJS 99, 701

Gerbaldi M., Floquet M., Faraggiana R., Van't Veer-Menneret C., 1989, A&AS 81, 127

Gliese W., 1982, A&AS 47, 471

Golub L., Harnden F.R. Jr., Maxson C.W., Rosner R., Vaiana G.S., 1983, ApJ 271, 264 (Errata: ApJ 278, 456)

Linsky J.L., 1990, in Imaging X-ray Astronomy, Elvis M. (ed.). Cambridge Univ. Press

Lockwood G.W., Thompson D.T., 1989, PASP 101, 705

Metanomski A.D.F., et al., 1997a (in preparation)

Metanomski A.D.F, Krautter J., Pasquini L., Cutispoto G., Fleming T.A., 1997b, Cool Stars, Stellar Systems and the Sun, Donahue R., Bookbinder J. (eds.) (in press)
Pallavicini R., Golub L., Rosner R., Vaiana G.S., Ayres T., Linsky J.L., 1981, ApJ 248, 279
Pallavicini R., 1989, A&AR 1, 177
Raga A.C., Mateo M., 1987, AJ 94, 684
Schmitt J.H.M.M., Fleming T.A., Giampapa M.S., 1995, ApJ 450, 392
Stocke J.T., Morris S.L., Gioia I.M., Maccacaro T., Schild R., Wolter A., Fleming T.A., Henry J.P., 1991, ApJS 76, 813
Trümper J., 1992, QJRAS 33, 165
Vaiana G.S., et al., 1981, ApJ 244, 163
Vaiana G.S., 1990, in Imaging X-ray Astronomy, Elvis M. (ed.). Cambridge Univ. Press
Vilhu O., Walter F.M., 1987, ApJ 321, 958
Voges W., 1992, in Space Sciences with Particular Emphasis on High-Energy Astrophysics, Guyenne T.D., Hunt J.J. (eds.)
Voges W., 1993, Adv. Space Res. 13, 391